ACS APPLIED MATERIALS & INTERFACES

Research Article

www.acsami.org

Enhanced Efficiency in Fullerene-Free Polymer Solar Cell by Incorporating Fine-designed Donor and Acceptor Materials

Long Ye, Kai Sun, Wei Jiang, Shaoqing Zhang, Wenchao Zhao, Huifeng Yao, Zhaohui Wang,* and Jianhui Hou*

Beijing National Laboratory for Molecular Sciences, Institute of Chemistry, Chinese Academy of Sciences, Beijing 100190, P. R. China

Supporting Information

ABSTRACT: Among the diverse nonfullerene acceptors, perylene bisimides (PBIs) have been attracting much attention due to their excellent electron mobility and tunable molecular and electronic properties by simply engineering the bay and head linkages. Herein, guided by two efficient small molecular acceptors, we designed, synthesized, and characterized a new nonfullerene small molecule PPDI with fine-tailored alkyl chains. Notably, a certificated PCE of 5.40% is realized in a simple structured fullerene-free polymer solar cell comprising PPDI as the electron acceptor and a fine-tailored 2D-conjugated polymer PBDT-TS1 as the electron donor. Moreover, the device behavior, morphological feature, and origin of high efficiency in PBDT-TS1/PPDI-based fullerene-free PSC were investigated. The synchronous selection and design of donor and acceptor materials reported here offer a feasible strategy for realizing highly efficient fullerene-free organic photovoltaics.

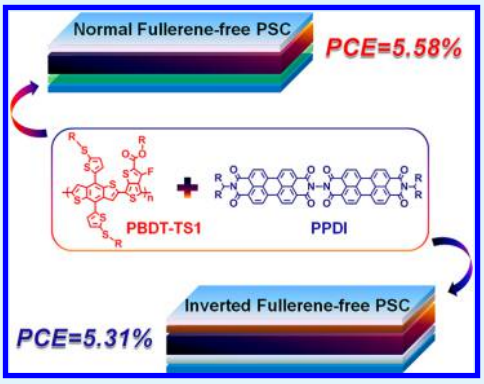

KEYWORDS: *polymer solar cells, perylene bisimides, nonfullerene acceptor, donor polymers*

1. INTRODUCTION

Fullerene-free polymer solar cells (PSCs) are emerging as potential applications in energy harvesting devices, in which the photoactive layers are typically comprised of conjugated polymers as electron donors and cost-effective nonfullerene materials,[1−19] like polymeric or small molecular materials as electron acceptors. Due to the higher optical and electronic variability, nonfullerene acceptors could afford excellent electron mobilities up to 10^{-3}−10^{-2} $cm^2V^{-1}s^{-1}$ and red-shifted absorption spectra covering 500−800 nm, which are comparable or even superior to those of fullerene acceptors.[1,19] The past two years have witnessed impressive advances in the power conversion efficiencies (PCEs) of fullerene-free PSCs. Nevertheless, these values are still lower than the values obtained from the PSCs based on the fullerene derivatives like [6,6]-phenyl-C_{71}-butyric acid methyl ester ($PC_{71}BM$). Therefore, fundamental understanding and efforts of the involved materials including both fullerene-free acceptors and polymer donors are still requisite to promote the PCEs of fullerene-free PSCs.

Among the diverse nonfullerene small molecular acceptors, perylene bisimides (PBIs) have been attracting much attention due to their excellent electron mobility and tunable molecular and electronic properties by simply modifying the attached alkyl chains or linkers.[20−29] The most remarkable aspect of these materials is that they can afford good short-circuit current denisty (J_{sc}) ranging from 8 to 12 mA/cm^2.[30−33] In 2012, Narayan and co-workers designed a nonplanar dimeric PBI derivative,[28] named as PPDI-1 (Scheme 1a), in which the twisted N—N single bond significantly reduced the planarity and thus the aggregation effect of acceptors was weakened. They applied PPDI-1 in the fullerene-free PSCs, and an encouraging PCE of ∼3% was obtained when it was blended with a 2D-conjugated polymer PBDTTT-C-T (Scheme 1b). The electrical, optical, and morphological studies further implied that PPDI-1 and its analogues should be a promising model system for efficient fullerene-free PSCs.[30] These studies have motivated the development of new strategies to produce dimeric PBIs with twisted structures. For instance, we very recently carried out detailed investigations of side chains of single-bond linked PBI dimers and found that the molecule with the alkyl chain C_5H_{11}, namely SDIPBI is the best one for photovoltaic application,[29] as summarized in Table 1, and moreover, SDIPBI also generated a few cases of impressive PCE surpassing 4.0% in normal and inverted geometry fullerene-free PSCs.[31,32] According to the reported works, it is interesting to note that only a slight difference in the length of alkyl chains results in a significant difference in their device performance. Considering that the PCEs for PPDI-1-based devices are still limited at 3.2% until now, we designed and synthesized a fine-optimized fullerene-free acceptor named as PPDI by replacing C_7H_{15} with C_5H_{11} in PPDI-1, as shown in Scheme 1a. Theoretical calculations verified the appropriate energy levels and nonplanar molecular conformation (Scheme 1c) of PPDI, in which the two PBI fragments are linked

Received: March 6, 2015
Accepted: April 16, 2015
Published: April 28, 2015

DOI: 10.1021/acsami.5b02012
ACS Appl. Mater. Interfaces 2015, 7, 9274−9280

Scheme 1. (a) Molecular Structure of Non-Fullerene Acceptors: SDIPBI-1, SDIPBI, PPDI-1, and PPDI; (b) Molecular Structure of Donor Polymers: PBDTTT-C-T and PBDT-TS1; (c) Schematic Illustration of the Molecular Geometry Optimization and Energy Levels of PPDI

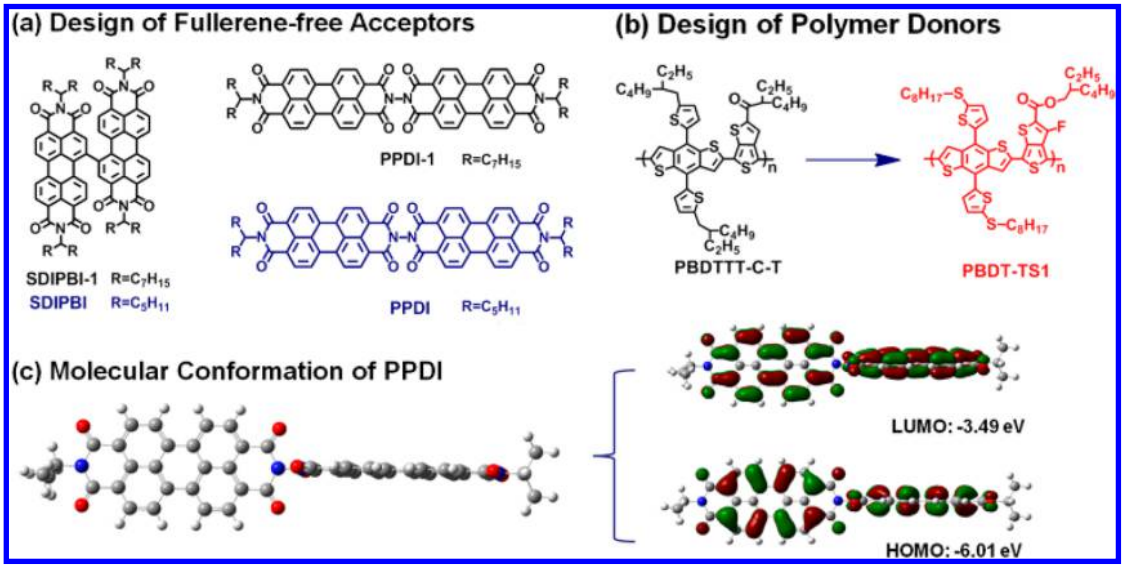

Table 1. Photovoltaic Parameters of Several Efficient Fullerene-Free PSCs

polymer	acceptor	V_{oc} [V]	J_{sc} [mA/cm^2]	*FF*	PCE [%]	ref.
PBDTTT-C-T	SDIPBI-1	0.72	8.86	0.40	2.54	29
PBDTTT-C-T	SDIPBI	0.73	10.58	0.47	3.63	28
PBDTTT-C-T	PPDI-1	0.77	9.00	0.46	3.20	30
PBDT-TS1	PPDI	0.82	12.51	0.53	5.40[a]	this work

[a]The certificated result from National Institute of Metrology (NIM), China.

perpendicularly to each other due to the repulsion of electron clouds on oxygen atoms. Additionally, for a conjugated molecule, the conjugated moiety is the key component for π-electron transport, while the nonconjugated alkyl chains ensure the solubility in processing solvents. Actually, the appended C_5H_{11} chains in PPDI can guarantee the solubility, the same as that of in SDIPBI. Therefore, reducing the ratio or length of the alkyl chains will be beneficial for optimizing the photovoltaic properties of PPDI.

Beyond structural modification of the nonfullerene acceptors, there also remain significant opportunities for improving the overall PCE of these promising acceptors by screening well-matched donor polymers.[17,18,24−28] In other words, the following criteria are required for donor polymers used in the highly efficient fullerene-free PSCs: (i) strong extinction coefficients and broad absorption spectra, (ii) formation of nanoscale and bicontinuous phase separation with fullerene-free acceptors, and (iii) high hole mobility and suitable energy level matching with nonfullerene acceptors. Lately, a novel 2D-conjugated BDT-based polymer with a deeper highest occupied molecular orbital (HOMO) level (−5.3 eV), namely PBDT-TS1[34] (see Scheme 1b) was designed, synthesized, and applied in fullerene-based PSC, which yielded a remarkable PCE exceeding 9% and undoubtedly outperformed PBDTTT-C-T[35] as donor polymers in PSCs. Herein, the simple structured fullerene-free PSCs employing the blend of PBDT-TS1/PPDI as the photoactive layer delivered a certificated PCE of 5.40%, which is nearly 2-fold of that obtained from the pristine PBDTTT-C-T/PPDI-1 system (Table 1). Furthermore, the device behaviors and morphological properties of the PBDT-TS1/PPDI system were investigated in detail.

2. EXPERIMENTAL SECTION

2.1. Preparation and Characterization of Materials. PPDI was synthesized following the similar route as reported by Narayan et al.[28] Compound PPDI: ^{1}H NMR ($CDCl_3$, 400 MHz, δ): 8.71 (d, 8H), 8.63 (d, 4H), 8.59 (d, 4H), 5.23−5.19 (m, 2H), 2.31−2.23 (m, 4H), 1.91−1.86 (m, 4H), 1.40−1.24 (m, 24H), 0.84 (t, 12H).^{13}C NMR ($CDCl_3$, 100 MHz, δ): 160.2, 135.3, 133.6, 132.3, 129.6, 129.2, 126.2, 126.0, 123.7, 122.7, 122.4, 55.0, 32.5, 31.9, 26.9, 22.8, 14.2. MS (HR-MALDI-TOF, see Supporting Information, SI, Figure S1): m/z (M^-) = 1086.458093 (calcd for $C_{70}H_{62}N_4O_8$: 1086.457314). PBDTTT-C-T (M_n = 20 K; PDI = 3.2), PBDT-TS1 (M_n = 29 K; PDI = 2.2), and SDIPBI were consistent with our previous reports. PFN was commercially available from Solarmer Material Inc. The processing solvents used in device fabrication process were purchased from Alfa Aesar. The PEDOT/PSS (Heraeus Clevios P VP AI 4083) and metal materials are commercially available products and used as received.

2.2. Fabrication and Characterization of PSC Devices. The D/A ratio is 1:1 for all of the polymer/acceptor blends following the device optimizations in previous works.[28−30] Other device fabrications details are provided in the SI. The $J-V$ characteristics were measured by a Keithley 2400 Source Measure Unit under the light intensity of AM1.5 G 100 mW/cm^2. The light intensity was calibrated using a silicon reference cell (with KG3 filter, purchased from Enli Technology Co. Ltd. and calibrated by NIM) to bring spectral mismatch factor to unity.[36] The typical active area of the certificated PSCs was about 5.65 mm^2, as defined by an optical microscope. The *EQE* curves were monitored by the use of the QE-R3011 Quantum Efficiency Equipment (Enli Technology Co. Ltd., Taiwan).

DOI: 10.1021/acsami.5b02012
ACS Appl. Mater. Interfaces 2015, 7, 9274−9280

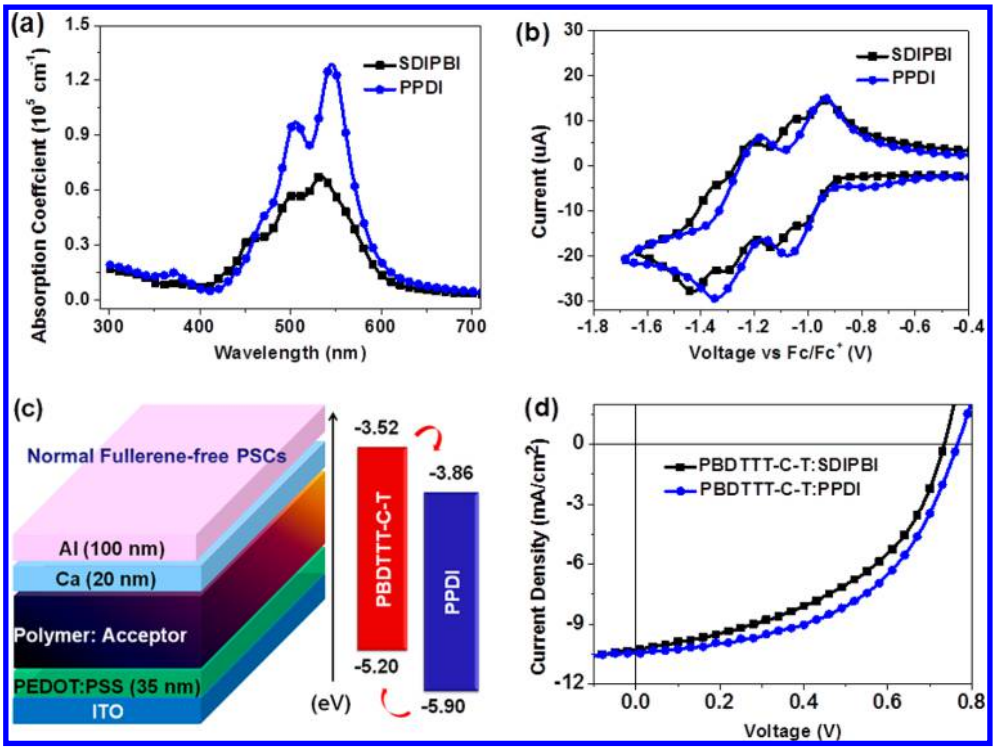

Figure 1. (a) UV−vis absorption spectra of PPDI and SDIPBI in thin films; (b) C−V plots of PPDI and SDIPBI; (c) schematic illustration of a normal device architecture; and (d) *J*−*V* curves of fullerene-free PSCs based on PBDTTT-C-T/SDIPBI and PBDTTT-C-T/PPDI blends.

Table 2. Photovoltaic Parameters of the Fullerene-Free PSC Devices

polymer	acceptor	V_{oc} [V]	J_{sc}[mA/cm^2]	*FF* [%]	PCE[a] [%]
PBDTTT-C-T	SDIPBI	0.72 ± 0.01	10.29 ± 0.18	0.45 ± 0.03	3.25 ± 0.17 (3.45)
PBDTTT-C-T	PPDI	0.76 ± 0.01	10.46 ± 0.26	0.49 ± 0.02	3.78 ± 0.15 (3.94)
PBDT-TS1	PPDI	0.80 ± 0.01	12.85 ± 0.23	0.53 ± 0.02	5.45 ± 0.12 (5.58)
PBDT-TS1[b]	PPDI	0.78 ± 0.02	13.14 ± 0.31	0.51 ± 0.02	5.09 ± 0.21 (5.31)

[a]Average values were calculated from about ten devices for each condition; the highest PCE values are shown in parentheses. [b]Values were obtained from inverted devices.

3. RESULTS AND DISCUSSION

PPDI is a linear dimer of PBI linked by a Nitrogen−Nitrogen single bond and could be facilely prepared by reacting imide anhydride and hydrazine adduct of PBIs with high yield according to the method.[28] The chemical structure of PPDI was carefully determined by NMR spectroscopy and mass spectrometry. PPDI shows a strong absorption in the range of 450−550 nm and a maximum molar extinction coefficient of 2.2×10^5 $M^{-1}cm^{-1}$ in chloroform solution (see SI Figure S2). To make clear comparisons of the basic properties like UV−vis absorption spectrum and cyclic voltammetry (CV) of PPDI in solid film, the corresponding data of SDIPBI were also characterized in parallel. It can be observed that these two acceptors exhibit similar spectral spectra from 300 to 600 nm (see Figure 1a), and their corresponding optical band gaps calculated from the absorption edge are approximately 2.04 eV. Compared to SDIPBI film, the absorption spectrum of PPDI film is slightly red-shifted (10 nm) and possesses a much higher absorption coefficient of 1.3×10^{-5} cm^{-1}. The high absorption capability should be ascribed to the reduced linearity and ratio of alkyl chains in the whole molecule as well as the relatively higher oscillator strength by DFT calculations. As shown in Figure 1b, the redox onset potentials of SDIPBI and PPDI are approximately 0.91 and 0.94 V, respectively. Consequently, the lowest unoccupied molecular orbital (LUMO) level of PPDI is determined to be −3.86 eV, which is 0.03 eV higher in comparison with that of SDIPBI. In addition, the electron mobilities of PPDI and SDIPBI were examined by the space-charge limit current (SCLC) method (SI Figure S3). The pristine film showed an electron mobility up to 4.1×10^{-4} $cm^2V^{-1}s^{-1}$ for PPDI, which is three times higher than that of SDIPBI. Obviously, these results indicated that PPDI is a potential replacement for SDIPBI in efficient fullerene-free PSCs.

Then, the photovoltaic performance of PPDI was evaluated by fabricating PSCs with a normal device architecture as illustrated in Figure 1c. Fullerene-free PSCs based on PBDTTT-C-T/SDIPBI were also fabricated as controls. The corresponding photovoltaic parameters of PBDTTT-C-T/PPDI and PBDTTT-C-T/SDIPBI were enumerated in Table 2. It can be observed that PBDTTT-C-T/PPDI based fullerene-free PSC delivers an average PCE of 3.78%, which is 17% higher than that of its SDIPBI-based device (3.25%) under the same conditions (see Figure 1d). Blending with PBDTTT-C-T, the newly designed PPDI possesses better photovoltaic performance (increased FF) over previous SDIPBI or PPDI-1. Encouraged by this preliminary result, it can be expected that

DOI: 10.1021/acsami.5b02012
ACS Appl. Mater. Interfaces 2015, 7, 9274−9280

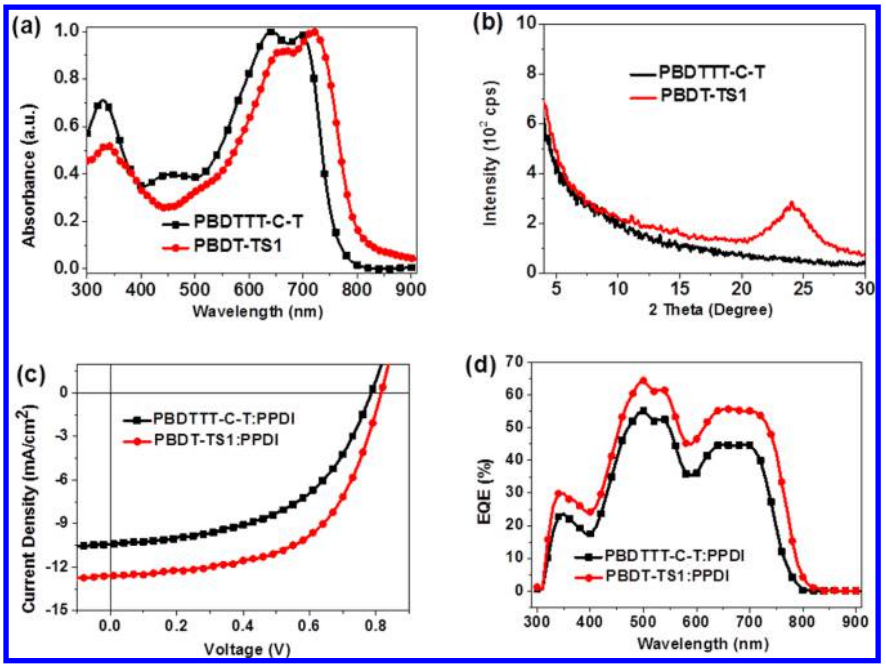

Figure 2. (a) UV−vis absorption and (b) XRD patterns of pure PBDTTT-C-T and PBDT-TS1 films; (c) *J*−*V* and (d) *EQE* curves of fullerene-free PSCs based on PBDTTT-C-T/PPDI and PBDT-TS1/PPDI blends.

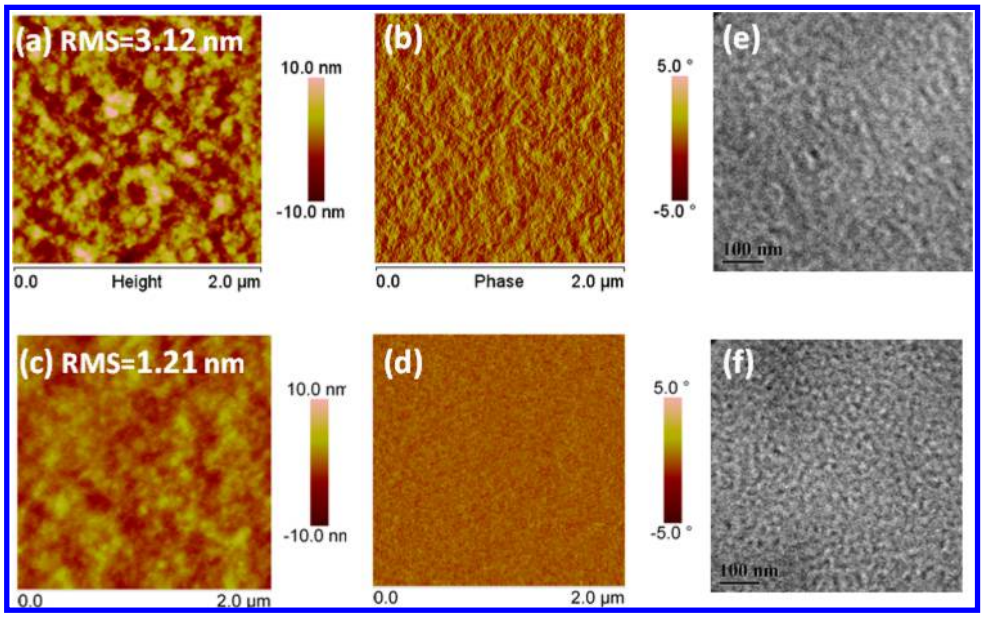

Figure 3. AFM and TEM images of fullerene-free PSCs based on PBDT-TS1/PPDI (a, b, e) and PBDTTT-C-T/PPDI (c, d, f) blend films.

higher efficiency will be realized by applying other well-matched donor polymers in the PPDI-based PSCs.

From the viewpoint of molecular design, PBDT-TS1 is a fine-optimized 2D-conjugated polymer, which has similar structure but better absorption spectrum compared to PBDTTT-C-T, and especially, it shows strong interchain $\pi-\pi$ stacking property than PBDTTT-C-T. As shown in Figure 2a, PBDT-TS1 exhibits an absorption range covering 300−820 nm, which is ca. 30 nm red-shifted compared to that of PBDTTT-C-T. However, the X-ray diffraction (XRD) patterns of the PBDT-TS1 film exhibits a clear $\pi-\pi$ stacking feature, while the film of PBDTTT-C-T shows much weaker $\pi-\pi$ stacking and no signal can be observed (Figure 2b). Additionally, the hole mobility of PBDT-TS1 (1×10^{-2} $cm^2V^{-1}s^{-1}$)[34] was found to be nearly 1 order of magnitude higher than that of PBDTTT-C-T (1.8×10^{-3} $cm^2V^{-1}s^{-1}$).[37] Consequently, the combination of high carrier mobility and broad spectral coverage as well as ordered packing render PBDT-TS1 attractive as donor material for high performance fullerene-free PSC applications.

According to the above results and considerations, there is still a lot of room to promote the efficiency of the fullerene-free PSCs based on PPDI by replacing PBDTTT-C-T with PBDT-TS1. Hence, the fullerene-free PSCs with conventional device architecture employing PBDT-TS1/PPDI as active layer were fabricated and characterized to afford an average PCE of 5.45% along with V_{oc} of 0.80 ± 0.01 V, J_{sc} of 12.85 ± 0.23 mA/cm^2, and FF of 0.53 ± 0.02 under AM 1.5 G illumination at the intensity of 100 mW/cm^2, as depicted in Figure 2c. One of the

DOI: 10.1021/acsami.5b02012
ACS Appl. Mater. Interfaces 2015, 7, 9274−9280

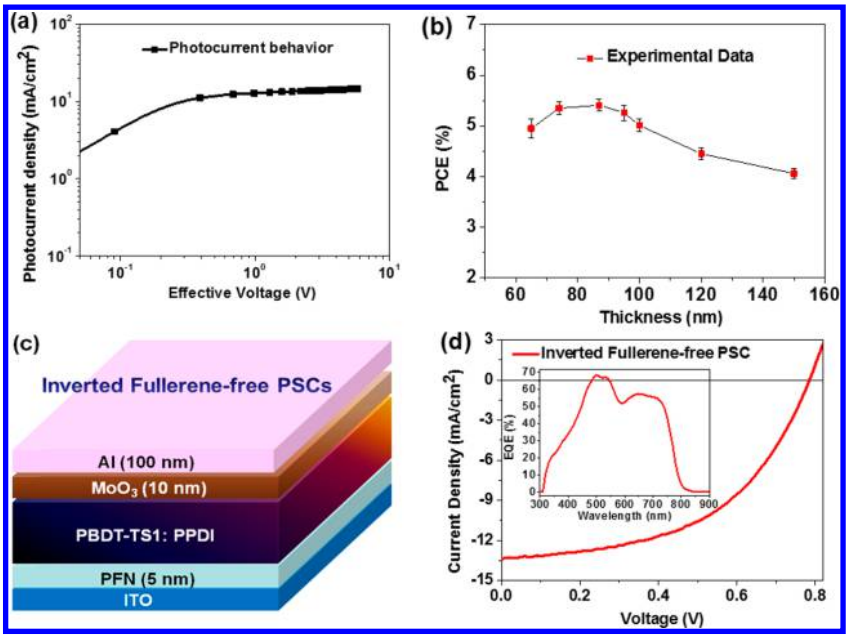

Figure 4. (a) The photocurrent vs effective voltage and (b) efficiency vs thickness plots of PBDT-TS1/PPDI-based conventional fullerene-free PSCs; (c) device geometry and (d) *J*−*V* curve of PBDT-TS1/PPDI-based inverted fullerene-free PSC. The insert image is the corresponding *EQE* curve.

best-performing fullerene-free PSCs was sent to the National Institute of Metrology (NIM) for certification, confirming a PCE of 5.40% with V_{oc} = 0.82 V, J_{sc} = 12.5 mA/cm^2, FF = 0.53 under the standard AM 1.5 G 100 mW/cm^2 condition (see SI Figure S4). Notably, the newly designed PBDT-TS1/PPDI system is one of very few fullerene-free combinations so far with efficiency up to 5.58% in PSCs. As shown in Figure 2d, the fullerene-free PSC device employing PBDT-TS1 exhibited a much broad photoresponse range from 300 to 820 nm. The wavelength integration of the product of the EQE curves and the standard AM 1.5G solar spectrum yields consistent J_{sc} values within 3% error compared to the results from *J*−*V* test. It is worth to note that the PBDT-TS1/PPDI based PSCs provides a maximum EQE of ∼65%, which is among the highest values reported so far and merely 15% lower than the peak EQE value in the corresponding PBDT-TS1/$PC_{71}BM$-based PSCs. The fullerene-free PSCs based on PBDTTT-C-T:PPDI were also fabricated and tested in parallel, and the best-performing device showed a V_{oc} of 0.76 V, a J_{sc} of 10.37 mA/cm^2, a FF of 0.50 and an overall PCE of 3.94%. Obviously, when the donor polymer was changed from PBDTTT-C-T to PBDT-TS1, the V_{oc}, J_{sc}, and FF of fullerene-free PSCs can be improved simultaneously.

To reveal the high current and PCE in PBDT-TS1/PPDI fullerene-free systems, atomic force microscopy (AFM) in a tapping mode was employed to probe the topography (Figure 3a) and phase morphologies of the blend films (Figure 3b). It can be observed that PBDT-TS1/PPDI blend film exhibited a higher root-mean-square roughness (RMS) of 3.12 nm and much clearer phase separation with an appropriate domain size of 20−30 nm, compared to that of PBDTTT-C-T/PPDI blend (Figure 3c,d). The RMS value of the PBDT-TS1/PPDI film is similar to the values obtained in previous cases of high-performance fullerene-free systems, for instance, PBDTBDD/SDIPBI[32] and PTB7-Th/SDIPBI[31] blends. In the PBDTTT-C-T/PPDI film, the very smooth surface and blurry phase separation might lead to severe bimolecular recombination, while in the PBDT-TS1/PPDI case, the obvious phase feature should be ascribed to the strong $\pi-\pi$ stacking effect of PBDT-TS1. Thus, the morphology of the PBDT-TS1/PPDI blend is more favorable than that of the PBDTTT-C-T/PPDI blend film from the AFM characterizations, and this should be an important factor contributed to the better EQE of the PBDT-TS1/PPDI device. The evolution of phase features from PBDTTT-C-T/PPDI (Figure 3e) to PBDT-TS1/PPDI (Figure 3f) blend film can be also confirmed in the transmission electron microscopy (TEM) images. Space charge limited current (SCLC) measurements and photocurrent analysis were conducted to probe the underlying physical processes like charge separation and transport characteristics. The PBDT-TS1/PPDI device shown a relatively balanced hole/electron mobility (μ_e = 1.2 × 10^{-3} and μ_h = 8.9 × 10^{-3} cm^{2}V^{-1}s^{-1}, respectively) according to the characterizations of hole-only and electron-only diodes of the blend films (SI Figure S5). Photocurrent behavior analysis (Figure 4a) revealed that the exciton dissociation efficiency is as high as 85.6% in the PBDT-TS1/PPDI blend, indicating efficient charge carrier output in the D/A interface.[10,32] Overall, it becomes apparent that the balance of electron/hole mobilities, efficient charge separation, and favorable phase separation must be related to the simultaneous increase in J_{sc} and FF of the PBDT-TS1/PPDI combination. The high dissociation efficiency in PBDT-TS1/PPDI-based PSC is comparable to that of some efficient fullerene-based photovoltaic devices, indicating that efficient exciton dissociation also exists in some polymer/fullerene-free acceptor systems.

To explore the potential of the PBDT-TS1/PPDI system for practical applications, the correlation between thickness and efficiency is carried out, as depicted in Figure 4b and SI Table S1. Interestingly, the PCE of PBDT-TS1/PPDI-based PSC is kept at ca. 5.2%, independent of the film thickness in the range of 60−100 nm. The fullerene-free PSC still attains a considerable PCE of 4.06% even with a thickness of 150 nm. Clearly, these features make the PBDT-TS1/PPDI-based

DOI: 10.1021/acsami.5b02012
ACS Appl. Mater. Interfaces 2015, 7, 9274−9280

fullerene-free PSC reproducible and compatible with the roll-to-roll printing technologies due to the requirement of over 100 nm-thick active layers. Apart from the conventional devices, inverted fullerene-free PSCs were also explored due to the excellent stability and performance.[37−40] The typical $J-V$ curve of the inverted fullerene-free PSC with a device geometry[40−42] of ITO/PFN/polymer/acceptor/MoO_3/Al (Figure 4c) was recorded in Figure 4d. The best-performing inverted devices based on PBDT-TS1/PPDI also exhibited a promising PCE of 5.31% with a V_{oc} of 0.79 V, a J_{sc} of 13.19 mA/cm^2 and a FF of 0.51. From these studies, we speculate that the successful application of PBDT-TS1 in PPDI-based PSCs with various architectures will greatly enhance the versatility of PBDT-TS1, not only for PBI-based small molecules, but also for other small molecule or polymer acceptors. The current device parameters in inverted fullerene-free PSCs might be meliorated by further engineering the n-type buffer layers, for instance, incorporating high quality C_{60}-SAM or ZnO,[31] which is out of the focus of this study.

In order to reveal the difference between fullerene-free PSC and fullerene-based PSC, the key parameters of PBDT-TS1/PPDI and PBDT-TS1/PC_{71}BM-based devices were listed in SI Table S2. Although the optimum D/A ratio and processing additives of the PBDT-TS1/PPDI blend are not identical to that of PBDT-TS1/PC_{71}BM system, we noted that the PBDT-TS1/PPDI blend film exhibits a similar morphology feature with that of the PBDT-TS1/PC_{71}BM blend film.[34] Due to the synergetic effect of binary solvent additives, the nanoscale morphology is greatly optimized compared with single additive.[32] For device optimizations of fullerene-free PSCs, the focus should be manipulating the aggregation and nanoscale phase separation to the length scale of exciton diffusion length.

4. CONCLUSIONS

To summarize, guided by two efficient small molecular acceptors, we designed, synthesized, and characterized a new nonfullerene small molecule PPDI with fine-tailored alkyl chains. When PBDTTT-C-T and PPDI were employed as polymer and acceptor, respectively, the PCE of the device is higher than that of the PBDTTT-C-T/PPDI-1 and PBDTTT-C-T/SDIPBI device, indicating that PPDI is a promising acceptor material for fullerene-free PSCs; then in order to further improve the PCE, PBDTTT-C-T was replaced by PBDT-TS1. Benefiting from the enhanced interchain $\pi-\pi$ stacking effect of the polymer, the blend of PBDT-TS1/PPDI show a relatively higher and symmetric hole and electron mobility. As a result, a high PCE of 5.58% (certificated as 5.40%) was obtained in the fullerene-free PSC based on PBDT-TS1/PPDI. Moreover, the device behaviors, morphological features, and origins of high efficiency in PBDT-TS1/PPDI-based fullerene-free PSCs were investigated. We believe that the synchronous selection and design of PBDT-TS1/PPDI system in this work can be seen as an useful example for molecular design of donor and acceptor materials toward highly efficient fullerene-free PSCs.

■ ASSOCIATED CONTENT

Supporting Information

Experimental details, synthesis routes, and characterizations of PPDI, electron-only mobility characterizations of SDIPBI and PPDI, certified report of PBDT-TS1/PPDI-based fullerene-free PSCs, and characteristics of hole-only and electron-only diodes of PBDT-TS1/PPDI and PBDTTT-C-T/PPDI. The Supporting Information is available free of charge on the ACS Publications website at DOI: 10.1021/acsami.5b02012.

■ AUTHOR INFORMATION

Corresponding Authors

*E-mail: zhaohuiwang@iccas.ac.cn (Z.W.).
*Tel: +86-10-82615900; e-mail: hjhzlz@iccas.ac.cn (J.H.).

Author Contributions

L.Y. and K.S. contributed equally in this work.

Notes

The authors declare no competing financial interest.

■ ACKNOWLEDGMENTS

For financial support of this research, we thank the National Basic Research Program 973 (Grants 2014CB643501 and 2013CB933500), NSFC (Grants 91333204, 51261160496, and 21225209, 91427303), NSFC-DFG Joint Project TRR61, and the Chinese Academy of Sciences (XDB12030200).

■ REFERENCES

(1) Lin, Y.; Zhan, X. Non-fullerene Acceptors for Organic Photovoltaics: An Emerging Horizon. *Mater. Horiz.* **2014**, *1*, 470−488.

(2) Tang, Z.; Liu, B.; Melianas, A.; Bergqvist, J.; Tress, W.; Bao, Q.; Qian, D.; Inganas, O.; Zhang, F. A New Fullerene-Free Bulk-Heterojunction System for Efficient High-Voltage and High-Fill Factor Solution-Processed Organic Photovoltaics. *Adv. Mater.* **2015**, *27*, 1900−1907.

(3) Zhou, E.; Cong, J.; Wei, Q.; Tajima, K.; Yang, C.; Hashimoto, K. All-Polymer Solar Cells from Perylene Diimide Based Copolymers: Material Design and Phase Separation Control. *Angew. Chem., Int. Ed.* **2011**, *50*, 2799−2803.

(4) Zhou, Y.; Kurosawa, T.; Ma, W.; Guo, Y.; Fang, L.; Vandewal, K.; Diao, Y.; Wang, C.; Yan, Q.; Reinspach, J.; Mei, J.; Appleton, A. L.; Koleilat, G. I.; Gao, Y.; Mannsfeld, S. C. B.; Salleo, A.; Ade, H.; Zhao, D.; Bao, Z. High Performance All-Polymer Solar Cell via Polymer Side-Chain Engineering. *Adv. Mater.* **2014**, *26*, 3767−3772.

(5) Deshmukh, K. D.; Qin, T.; Gallaher, J. K.; Liu, A. C. Y.; Gann, E.; O'Donnell, K.; Thomsen, L.; Hodgkiss, J. M.; Watkins, S. E.; McNeill, C. R. Performance, Morphology and Photophysics of High Open-Circuit Voltage, Low Band Gap All-Polymer Solar Cells. *Energy Environ. Sci.* **2015**, *8*, 332−342.

(6) McNeill, C. R.; Greenham, N. C. Conjugated-Polymer Blends for Optoelectronics. *Adv. Mater.* **2009**, *21*, 3840−3850.

(7) Facchetti, A. Polymer Donor−Polymer Acceptor (All-Polymer) Solar Cells. *Mater. Today* **2013**, *16*, 123−132.

(8) Lee, C.; Kang, H.; Lee, W.; Kim, T.; Kim, K.-H.; Woo, H. Y.; Wang, C.; Kim, B. J. High-Performance All-Polymer Solar Cells Via Side-Chain Engineering of the Polymer Acceptor: The Importance of the Polymer Packing Structure and the Nanoscale Blend Morphology. *Adv. Mater.* **2015**, DOI: 10.1002/adma.201405226.

(9) Holliday, S.; Ashraf, R. S.; Nielsen, C. B.; Kirkus, M.; Rohr, J. A.; Tan, C. H.; Collado-Fregoso, E.; Knall, A. C.; Durrant, J. R.; Nelson, J.; McCulloch, I. A Rhodanine Flanked Nonfullerene Acceptor for Solution-Processed Organic Photovoltaics. *J. Am. Chem. Soc.* **2015**, *137*, 898−904.

(10) Liu, Y.; Mu, C.; Jiang, K.; Zhao, J.; Li, Y.; Zhang, L.; Li, Z.; Lai, J. Y.; Hu, H.; Ma, T.; Hu, R.; Yu, D.; Huang, X.; Tang, B. Z.; Yan, H. A Tetraphenylethylene Core-Based 3D Structure Small Molecular Acceptor Enabling Efficient Non-Fullerene Organic Solar Cells. *Adv. Mater.* **2015**, *27*, 1015−1020.

(11) Li, W.; Roelofs, W. S. C.; Turbiez, M.; Wienk, M. M.; Janssen, R. A. J. Polymer Solar Cells with Diketopyrrolopyrrole Conjugated Polymers as the Electron Donor and Electron Acceptor. *Adv. Mater.* **2014**, *26*, 3304−3309.

(12) Earmme, T.; Hwang, Y.-J.; Subramaniyan, S.; Jenekhe, S. A. All-Polymer Bulk Heterojuction Solar Cells with 4.8% Efficiency Achieved

DOI: 10.1021/acsami.5b02012
ACS Appl. Mater. Interfaces 2015, 7, 9274−9280

by Solution Processing from a Co-Solvent. *Adv. Mater.* **2014**, *26*, 6080−6085.
(13) Zhou, E.; Cong, J.; Hashimoto, K.; Tajima, K. Control of Miscibility and Aggregation via the Material Design and Coating Process for High-Performance Polymer Blend Solar Cells. *Adv. Mater.* **2013**, *25*, 6991−6996.
(14) Mori, D.; Benten, H.; Okada, I.; Ohkita, H.; Ito, S. Highly Efficient Charge-carrier Generation and Collection in Polymer/Polymer Blend Solar Cells with a Power Conversion Efficiency of 5.7%. *Energy Environ. Sci.* **2014**, *7*, 2939−2943.
(15) Zhou, Y.; Ding, L.; Shi, K.; Dai, Y. Z.; Ai, N.; Wang, J.; Pei, J. A Non-Fullerene Small Molecule as Efficient Electron Acceptor in Organic Bulk Heterojunction Solar Cells. *Adv. Mater.* **2012**, *24*, 957−961.
(16) Kang, H.; Uddin, M. A.; Lee, C.; Kim, K.-H.; Nguyen, T. L.; Lee, W.; Li, Y.; Wang, C.; Woo, H. Y.; Kim, B. J. Determining the Role of Polymer Molecular Weight for High-Performance All-Polymer Solar Cells: Its Effect on Polymer Aggregation and Phase Separation. *J. Am. Chem. Soc.* **2015**, *137*, 2359−2365.
(17) Lin, Y.; Wang, J.; Zhang, Z. G.; Bai, H.; Li, Y.; Zhu, D.; Zhan, X. An Electron Acceptor Challenging Fullerenes for Efficient Polymer Solar Cells. *Adv. Mater.* **2015**, *27*, 1170−1174.
(18) Pho, T. V.; Toma, F. M.; Tremolet de Villers, B. J.; Wang, S.; Treat, N. D.; Eisenmenger, N. D.; Su, G. M.; Coffin, R. C.; Douglas, J. D.; Fréchet, J. M. J.; Bazan, G. C.; Wudl, F.; Chabinyc, M. L. Decacyclene Triimides: Paving the Road to Universal Non-Fullerene Acceptors for Organic Photovoltaics. *Adv. Energy Mater.* **2014**, *4*, 1301426.
(19) Eftaiha, A. a. F.; Sun, J.-P.; Hill, I. G.; Welch, G. C. Recent Advances of Non-fullerene, Small Molecular Acceptors for Solution Processed Bulk Heterojunction Solar Cells. *J. Mater. Chem. A* **2014**, *2*, 1201−1213.
(20) Howard, I. A.; Laquai, F.; Keivanidis, P. E.; Friend, R. H.; Greenham, N. C. Perylene Tetracarboxydiimide as an Electron Acceptor in Organic Solar Cells: A Study of Charge Generation and Recombination. *J. Phys. Chem. C* **2009**, *113*, 21225−21232.
(21) Hartnett, P. E.; Timalsina, A.; Matte, H. S. S. R.; Zhou, N.; Guo, X.; Zhao, W.; Facchetti, A.; Chang, R. P. H.; Hersam, M. C.; Wasielewski, M. R.; Marks, T. J. Slip-Stacked Perylenediimides as an Alternative Strategy for High Efficiency Nonfullerene Acceptors in Organic Photovoltaics. *J. Am. Chem. Soc.* **2014**, *136*, 16345−16356.
(22) Sharenko, A.; Gehrig, D.; Laquai, F.; Nguyen, T.-Q. The Effect of Solvent Additive on the Charge Generation and Photovoltaic Performance of a Solution-Processed Small Molecule:Perylene Diimide Bulk Heterojunction Solar Cell. *Chem. Mater.* **2014**, *26*, 4109−4118.
(23) Zheng, Y.-Q.; Dai, Y.-Z.; Zhou, Y.; Wang, J.-Y.; Pei, J. Rational Molecular Engineering towards Efficient Non-fullerene Small Molecule Acceptors for Inverted Bulk Heterojunction Organic Solar Cells. *Chem. Commun.* **2014**, *50*, 1591−1594.
(24) Singh, R.; Aluicio-Sarduy, E.; Kan, Z.; Ye, T.; MacKenzie, R. C. I.; Keivanidis, P. E. Fullerene-free Organic Solar Cells with an Efficiency of 3.7% Based on a Low-Cost Geometrically Planar Perylene Diimide Monomer. *J. Mater. Chem. A* **2014**, *2*, 14348−14353.
(25) Zhang, X.; Lu, Z.; Ye, L.; Zhan, C.; Hou, J.; Zhang, S.; Jiang, B.; Zhao, Y.; Huang, J.; Zhang, S.; Liu, Y.; Shi, Q.; Liu, Y.; Yao, J. A Potential Perylene Diimide Dimer-Based Acceptor Material for Highly Efficient Solution-Processed Non-Fullerene Organic Solar Cells with 4.03% Efficiency. *Adv. Mater.* **2013**, *25*, 5791−5797.
(26) Zhong, Y.; Trinh, M. T.; Chen, R.; Wang, W.; Khlyabich, P. P.; Kumar, B.; Xu, Q.; Nam, C.-Y.; Sfeir, M. Y.; Black, C.; Steigerwald, M. L.; Loo, Y.-L.; Xiao, S.; Ng, F.; Zhu, X. Y.; Nuckolls, C. Efficient Organic Solar Cells with Helical Perylene Diimide Electron Acceptors. *J. Am. Chem. Soc.* **2014**, *136*, 15215−15221.
(27) Li, H.; Earmme, T.; Ren, G.; Saeki, A.; Yoshikawa, S.; Murari, N. M.; Subramaniyan, S.; Crane, M. J.; Seki, S.; Jenekhe, S. A. Beyond Fullerenes: Design of Nonfullerene Acceptors for Efficient Organic Photovoltaics. *J. Am. Chem. Soc.* **2014**, *136*, 14589−14597.
(28) Rajaram, S.; Shivanna, R.; Kandappa, S. K.; Narayan, K. S. Nonplanar Perylene Diimides as Potential Alternatives to Fullerenes in Organic Solar Cells. *J. Phys. Chem. Lett.* **2012**, *3*, 2405−2408.
(29) Jiang, W.; Ye, L.; Li, X.; Xiao, C.; Tan, F.; Zhao, W.; Hou, J.; Wang, Z. Bay-Linked Perylene Bisimides as Promising Non-fullerene Acceptors for Organic Solar Cells. *Chem. Commun.* **2014**, *50*, 1024−1026.
(30) Shivanna, R.; Shoaee, S.; Dimitrov, S.; Kandappa, S. K.; Rajaram, S.; Durrant, J. R.; Narayan, K. S. Charge Generation and Transport in Efficient Organic Bulk Heterojunction Solar Cells with a Perylene Acceptor. *Energy Environ. Sci.* **2014**, *7*, 435−441.
(31) Zang, Y.; Li, C.-Z.; Chueh, C.-C.; Williams, S. T.; Jiang, W.; Wang, Z.-H.; Yu, J.-S.; Jen, A. K. Y. Integrated Molecular, Interfacial, and Device Engineering towards High-Performance Non-Fullerene Based Organic Solar Cells. *Adv. Mater.* **2014**, *26*, 5708−5714.
(32) Ye, L.; Jiang, W.; Zhao, W.; Zhang, S.; Qian, D.; Wang, Z.; Hou, J. Selecting a Donor Polymer for Realizing Favorable Morphology in Efficient Non-fullerene Acceptor-Based Solar Cells. *Small* **2014**, *10*, 4658−4663.
(33) Zhang, X.; Zhan, C.; Yao, J. Non-Fullerene Organic Solar Cells with 6.1% Efficiency through Fine-Tuning Parameters of the Film-Forming Process. *Chem. Mater.* **2014**, *27*, 166−173.
(34) Ye, L.; Zhang, S.; Zhao, W.; Yao, H.; Hou, J. Highly Efficient 2D-Conjugated Benzodithiophene-Based Photovoltaic Polymer with Linear Alkylthio Side Chain. *Chem. Mater.* **2014**, *26*, 3603−3605.
(35) Huo, L. J.; Zhang, S. Q.; Guo, X.; Xu, F.; Li, Y. F.; Hou, J. H. Replacing Alkoxy Groups with Alkylthienyl Groups: A Feasible Approach To Improve the Properties of Photovoltaic Polymers. *Angew. Chem., Int. Ed.* **2011**, *50*, 9697−9702.
(36) Ye, L.; Zhou, C.; Meng, H.; Wu, H.-H.; Lin, C.-C.; Liao, H.-H.; Zhang, S.; Hou, J. Toward Reliable and Accurate Evaluation of Polymer Solar Cells Based on Low Band Gap Polymers. *J. Mater. Chem. C* **2015**, *3*, 564−569.
(37) Li, X. H.; Choy, W. C. H.; Huo, L. J.; Xie, F. X.; Sha, W. E. I.; Ding, B. F.; Guo, X.; Li, Y. F.; Hou, J. H.; You, J. B.; Yang, Y. Dual Plasmonic Nanostructures for High Performance Inverted Organic Solar Cells. *Adv. Mater.* **2012**, *24*, 3046−3052.
(38) Liu, Y.; Zhao, J.; Li, Z.; Mu, C.; Ma, W.; Hu, H.; Jiang, K.; Lin, H.; Ade, H.; Yan, H. Aggregation and Morphology Control Enables Multiple Cases of High-Efficiency Polymer Solar Cells. *Nat. Commun.* **2014**, *5*, 5293.
(39) Tseng, W.-H.; Chen, H.-C.; Chien, Y.-C.; Liu, C.-C.; Peng, Y.-K.; Wu, Y.-S.; Chang, J.-H.; Liu, S.-H.; Chou, S.-W.; Liu, C.-L.; Chen, Y.-H.; Wu, C.-I.; Chou, P.-T. Comprehensive Study of Medium-Bandgap Conjugated Polymer Merging a Fluorinated Quinoxaline with Branched Side Chains for Highly Efficient and Air-Stable Polymer Solar Cells. *J. Mater. Chem. A* **2014**, *2*, 20203−20212.
(40) He, Z.; Xiao, B.; Liu, F.; Wu, H.; Yang, Y.; Xiao, S.; Wang, C.; Russell, T. P.; Cao, Y. Single-Junction Polymer Solar Cells with High Efficiency and Photovoltage. *Nat. Photonics* **2015**, *9*, 174−179.
(41) Zhang, K.; Zhong, C.; Liu, S.; Mu, C.; Li, Z.; Yan, H.; Huang, F.; Cao, Y. Highly Efficient Inverted Polymer Solar Cells Based on a Cross-linkable Water-/Alcohol-Soluble Conjugated Polymer Interlayer. *ACS Appl. Mater. Interfaces* **2014**, *6*, 10429−10435.
(42) Guo, X.; Zhang, M.; Ma, W.; Ye, L.; Zhang, S.; Liu, S.; Ade, H.; Huang, F.; Hou, J. Enhanced Photovoltaic Performance by Modulating Surface Composition in Bulk Heterojunction Polymer Solar Cells Based on PBDTTT-C-T/$PC_{71}BM$. *Adv. Mater.* **2014**, *26*, 4043−4049.

DOI: 10.1021/acsami.5b02012
ACS Appl. Mater. Interfaces 2015, 7, 9274−9280